



Alignment of orientation-modulated textures

Nicolaas Prins *, Alexander J. Mussap

School of Psychology, Deakin University, 221 Burwood Highway, Melbourne 3125, Australia

Received 11 February 2000; received in revised form 11 July 2000

Abstract

We conducted a Vernier acuity experiment using orientation-modulated (OM) textures in which the overall shape (skewness) of the modulations was manipulated independently of their orientation content. Misalignments between OMs were consistent with the application of global positional tags, but not on the basis of a single cue (e.g. centroid, peak, or zero-crossing). Instead, modelling of our results in terms of orientation-opponent spatial filters not only led to an excellent fit, but also to estimates of the size and shape of these filters that correspond closely to those made by other researchers using a different task and different stimulus parameters and configurations. © 2000 Elsevier Science Ltd. All rights reserved.

Keywords: Orientation modulation; Centroid analysis; Texture perception; Vernier acuity; Spatial filters

1. Introduction

Our ability to detect misalignments between stimuli separated by more than several min arc is surprisingly robust to differences in stimulus properties (O'Shea & Mitchell, 1990; Waugh & Levi, 1993; Toet & Koenderink, 1988; Levi & Klein, 1990). This has been taken as evidence for the theory of local signs in which underlying spatial filters are positionally labelled (Lotze, 1885; Westheimer & McKee, 1977). To explain accurate alignment performance it has been proposed that local positional signs can be integrated across space, for example, along the length of the stimuli to be aligned (Westheimer, 1981; Morgan & Glennerster, 1991).

Various criteria have been explored that could be used by the visual system to assign positional signs to spatial distributions of luminance or contrast elements, including the peak, the centroid, and/or the zero-crossings in the second derivative of the distributions (Akutsu, McGraw, & Levi, 1999; Badcock, Hess, & Dobbins, 1996; Hess & Holliday, 1992, 1996; Hess & Hayes, 1994; Whitaker, McGraw, Pacey & Barrett,

1996; Whitaker & McGraw, 1998). The general finding is that the perceived global position corresponds closely to the centroid of the distribution with varying degrees of paradigm-dependent bias determined by such factors as the midpoint of the distribution (the average position of the two visible spatial extremes along the axis of modulation; Badcock et al., 1996; Hess & Holliday, 1996), the peak of the distribution (Akutsu et al., 1999) or the zero-crossings (Akutsu et al., 1999).

The present series of experiments extended the above research on luminance, contrast, and colour to the orientation domain where the stimuli to be localised and aligned were orientation-modulated (OM) textures. Previous research on OM perception has indicated the involvement of processes that integrate orientation information over space, raising the possibility that OMs are detected and coded for explicitly by spatial filters tuned to second-order, orientation-defined structure (Arsenault, Wilkinson, & Kingdom, 1999; Kingdom, Keeble, & Moulden, 1995; Kingdom & Keeble, 1996). This idea is consistent with the discovery of neurones with orientation-opponent properties in primate areas V1 and MT (Knierim & Van Essen, 1992; Olavarria, DeYoe, Knierim, Fox & Van Essen, 1992).

It is reasonable to suppose that orientation-opponent filters are positionally labelled and able to code for the location of an OM within a background of otherwise

* Corresponding author. Tel.: +61-3-92446114; fax: +61-3-92446858.

E-mail address: nprins@deakin.edu.au (N. Prins).

uniform orientation. This idea is illustrated in Fig. 1. The left panel shows two OM textures (A) with their orientation profiles (B). In the middle panel a schematic representation of an orientation-opponent spatial filter is represented (C) together with its receptive-field profile (D). The right panel (E, F) shows the result of convolution of the two profiles which corresponds to the relative activation of a series of such filters as a function of retinotopic location along the axis of modulation of the OM, relative to the peak of the OM. The global location of the OM can then simply be taken as the position where maximum filter activation occurs.

In the present experiments pairs of textures were produced by filtering random noise with 2-D filters of narrowband orientation and spatial frequency. Rotating these filters in orientation along the horizontal axis according to a Gaussian function produced OMs of these textures. This method of construction allowed independent control of each OM's 'baseline' orientation (determined by the start and end orientation positions of the 2-D filter), as well as each OM's orientation at the peak of the modulation (determined by the direction and degree of rotation of the 2-D filter). The subjects' task was to align the two OMs along the vertical axis.

The critical variable, manipulated for one of the OMs in a pair, was the degree of similarity between the standard deviations of the left and right sides of the Gaussian distributions describing the shape of the OM. If the position of OMs is coded by the relative activation of orientation-opponent spatial filters as outlined above, it follows that the perceived location of the skewed OMs should be shifted in a predictable and testable manner (see right panel of Fig. 1). Furthermore, there should be no effect of the OM's baseline orientation nor of the direction and amplitude of the modulation, since the OM-specific filters code only for the orientation gradient, independent of absolute orientation content.

The results obtained demonstrate that observers are able to localise orientation gradients. The effects of manipulating the shape of orientation distributions are not readily explained by the use of any single location cue (such as the centroid, peak, or zero-crossing). However, modelling these effects via a bank of orientation-opponent filters leads to an excellent fit, with corresponding estimates of filter size and shape matching closely those derived from studies of OM transfer functions (cf. Kingdom & Keeble, 1996).

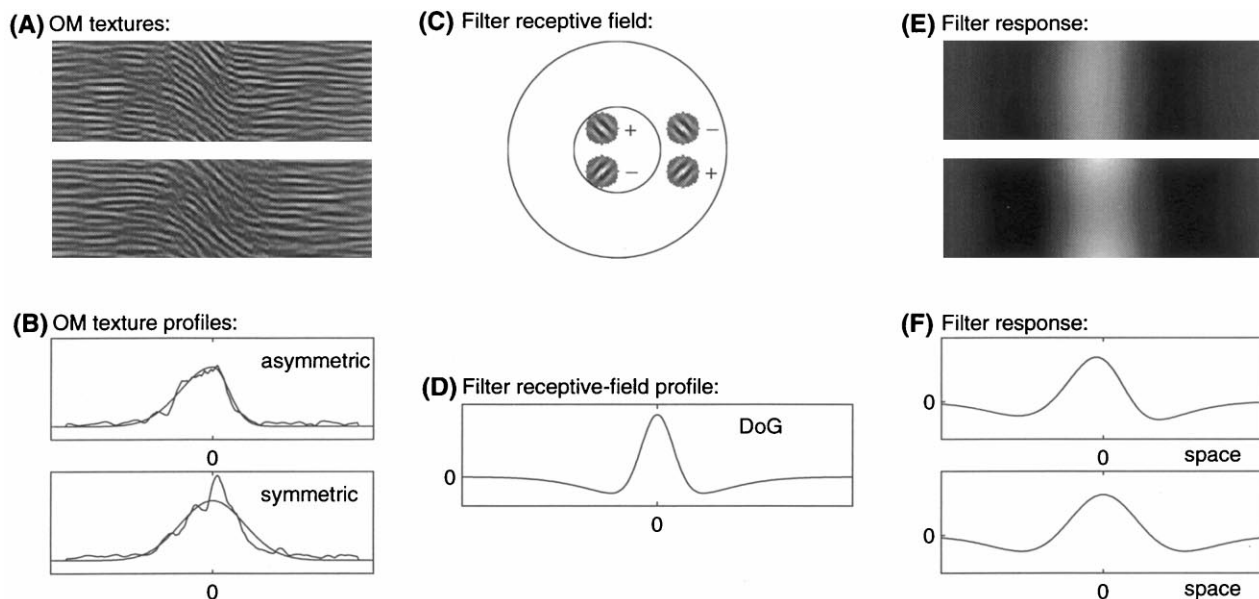


Fig. 1. Determining the location of an OM texture using orientation-opponent filters. The left panel shows two OM textures (A) which differ in their orientation profiles (B). Shown in (B) are both the stimulus generating functions (Section 2) as well as the orientation distributions as determined by filtering the textures in (A) with a Gabor filter centred at the peak spatial frequency of the stimulus and with relative spatial dimensions as proposed by Daugman (1980), followed by full-wave rectification and averaging within the vertical columns. (C) The receptive field of a putative orientation-opponent filter together with its receptive-field profile (D, modelled here as a Difference of Gaussians [DoG] function) is maximally sensitive to OMs which contain left-oblique orientations in the centre, and right-oblique orientations in the surround. The right panels (E, F) present the relative output of a set of these filters, aligned along the axis of orientation modulation, when presented with the stimulus in the left panel. As is clear from the figure, the location corresponding to maximum activation of these filters is shifted away from the peak orientation in case of the asymmetric OM.

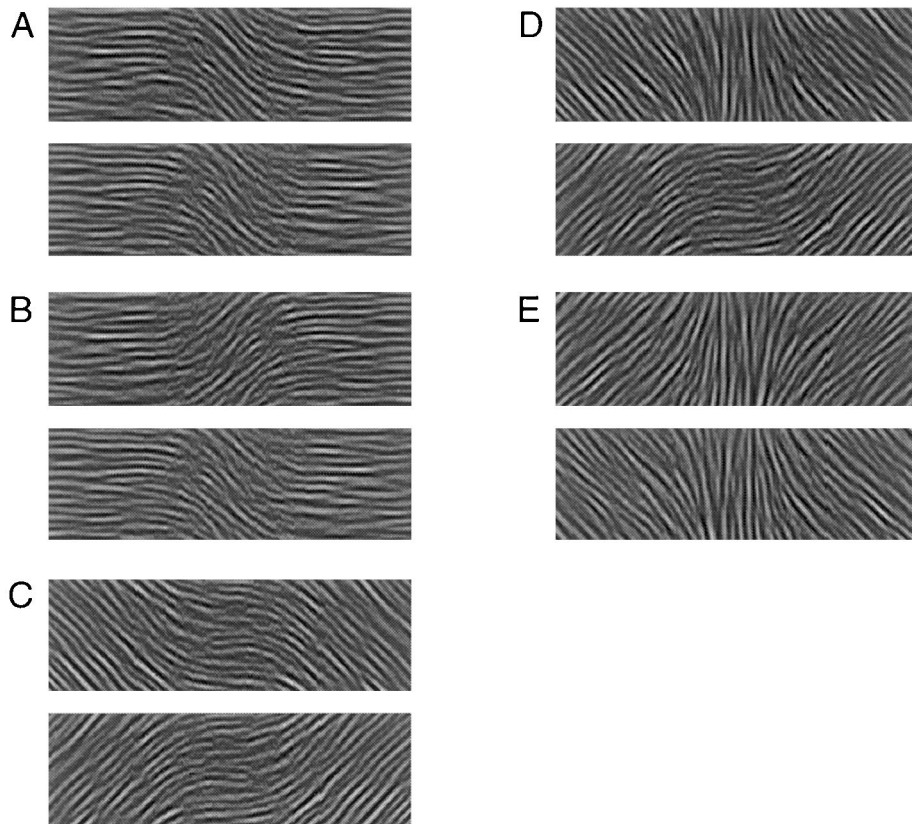


Fig. 2. The different stimulus configurations employed in the experiment. The orientation profile in these textures is described by a Gaussian function: $\theta_x = \theta_{\text{base}} + \theta_{\text{mod}} \cdot \exp(-x^2/[2 \cdot \sigma_{L/R}^2])$, where θ_{base} and θ_{mod} are as described in Table 1. All five configurations are shown here with symmetric profiles ($\sigma_L = \sigma_R$) and vertically aligned. The stimuli as presented here are not gamma-corrected.

2. Methods

2.1. Observers

Observers were the authors and a practised naive observer.

2.2. Apparatus and stimuli

Stimuli were presented on a 21 in. EIZO high-resolution monochrome monitor at a viewing distance of 1.5 m, gamma corrected to 32 000 grey levels (from 0 to 55 cd m^{-2}) via a Visionworks™ calibration system. These stimuli were generated by a Cambridge Research Systems™ CRS2/3F board, which was controlled by custom-written C-programs based on Visionworks™ graphics routines.

The stimuli consisted of pairs of 2-D filtered noise textures ($2.81 \times 0.89^\circ$ each), vertically separated by a 0.14° gap (Fig. 2). The filters were of narrowband spatial frequency (bandwidth $10.8 \text{ cyc deg}^{-1}$, centred at $12.6 \text{ cyc deg}^{-1}$ visual arc) and orientation (bandwidth = 20°). The orientation of these filters was modulated along the horizontal axis according to a Gaussian function. In all cases, the Gaussian function describing the modulation in the lower (reference) texture was

symmetrical ($\sigma = 16.6 \text{ min arc}$), whereas the upper (target) texture was modulated according to a Gaussian function with various degrees of asymmetry. The asymmetry was introduced by varying the standard deviation on either the left (σ_L) or right side (σ_R) of the peak (Whitaker et al., 1996) from 8.3 to 16.6 min arc in five equal steps, while the contralateral standard deviation remained fixed at 16.6 min arc. Base orientation and the direction of rotation of the modulation were varied to form five different configurations (Table 1 and Fig. 2), allowing us to (i) generalise results across different orientations, and (ii) vary the similarity between the upper and lower OMs in terms of the orientation present at the base, peak and zero-crossings of the OMs.

2.3. Procedure

The five configurations displayed in Table 1 and Fig. 2 were presented at the five degrees of asymmetry, leading to a total of 25 different stimulus conditions. The observers' task was to indicate, after each presentation, whether the upper OM appeared to the left or right of the lower OM. Within a block the base orientation and direction of modulation of the target and reference textures, as well as the degree of asymmetry

$(|\sigma_L - \sigma_R|)$, were held constant. The direction of asymmetry (the sign of $\sigma_L - \sigma_R$), however, was randomised within a block.

Alignment settings were determined according to an adaptive maximum-likelihood procedure (the Best PEST; Pentland, 1980). One block of trials consisted of six independent, randomly interleaved, PEST staircases (either three in which $\sigma_L < \sigma_R$ and three in which $\sigma_L > \sigma_R$, or all six in which $\sigma_L = \sigma_R$) of 30 trials each. The overall position of the reference OM was randomly jittered from trial to trial between -12 and $+12$ min from the centre of the stimulus. The presentation duration was 250 ms. No feedback was provided.

3. Results and discussion

The perceived position of the target OM relative to the reference OM was defined to be $(\mu_L - \mu_R)/2$, where μ_L (μ_R) is the mean of the alignment settings when σ_L (σ_R) was varied. This measure effectively removes any left/right response biases. When $\sigma_L = \sigma_R$, μ_L and μ_R were undefined and we defined $(\mu_L - \mu_R)/2$ to be zero. In Fig. 3, $(\mu_L - \mu_R)/2$ is plotted as a function of $|\sigma_L - \sigma_R|$, along with the response bias of observers, defined as $(\mu_L + \mu_R)/2$.

Inspection of the figure reveals that observers were able to detect and localise OM patterns. Clearly, they were also sensitive to the shape of the OM distribution over space, with perceived alignments shifted towards the direction of OM skew as an increasing function of the magnitude of the skew. Furthermore, the results suggest that OM shape was the only cue used by observers in making their judgements even though at least two other cues were available. For example, in some conditions observers could have made accurate

and consistent responses by aligning carrier orientations, either the orientation(s) of the base (Fig. 2A and B) and/or the orientation(s) of the peak (Fig. 2A, C, and E) of the OM carrier. However, our results show that observers were insensitive to the absolute orientation content of the OM patterns in that they made similar responses to all stimulus conditions. Consequently, we collapsed across base and peak conditions in subsequent analyses and include the combined data in Fig. 4.

Given the importance of OM shape in explaining our results it is worth considering which aspect of OM shape is important. Predictions from the most likely candidates, the peak, centroid and zero-crossings, are included in Fig. 4. Our results do not correspond to the use of any of these cues alone, but instead consistently fall midway between the centroid and zero-crossing predictions. Therefore, we considered the possibility that our results reflect an approximately equal contribution from both centroid and zero-crossing information because both are features of a single underlying type of spatial filter. We were also motivated by recent successful attempts at modelling OM detectability on the basis of filters sensitive to orientation contrast (Kingdom & Keeble, 1996; Gray & Regan, 1998), and by the discovery of visual neurones with orientation-opponent response profiles (Knierim & Van Essen, 1992; Olavarria et al., 1992) to interpret our results in terms of these filters.

To explore this issue further we attempted to model the size and shape of the putative orientation-opponent filters that best account for our OM localisation results, at least for the particular carrier spatial-frequency employed. By making the assumption that these filters are positionally labelled, the perceived position of an OM can simply be taken to be the retinal location of maximum excitation of these filters (see Fig. 1). We approximated the profile of the orientation-opponent receptive field by a balanced Difference-of-Gaussians (DoG) function:

$$\text{DoG} = \exp(-x^2/2\sigma_1^2) - (\sigma_1/\sigma_2) \exp(-x^2/2\sigma_2^2) \quad (1)$$

The choice of this function was motivated by its resemblance to the receptive field profiles estimated by Kingdom and Keeble (1996) as well as to the shape of cortical receptive fields (e.g. Marr & Ullman, 1981). The parameters of interest were σ_1 and σ_2 , which determine the overall size and shape of the function in Eq. (1). We estimated these parameters for our observers individually by generating predictions based on a range of values for σ_1 and σ_2 , and selecting those values for σ_1 and σ_2 which yielded the closest fit to the observers' data (using a least squares criterion). The predictions were generated by convolving the generative function of the stimulus orientation profile (Fig. 1B) with the profile of a DoG filter (Fig. 1D) and

Table 1
Configuration of the stimuli^a

Condition	Target (upper) OM		Reference (lower) OM	
	θ_{base}	θ_{mod}	θ_{base}	θ_{mod}
A	90	+45	90	+45
B	90	-45	90	+45
C	135	-45	45	+45
D	135	+45	45	+45
E	45	-45	135	+45

^a Orientation was modulated according to a Gaussian function: $\theta_x = \theta_{\text{base}} + \theta_{\text{mod}} \cdot \exp(-x^2/[2 \cdot \sigma_{L/R}^2])$. A pictorial representation of these stimuli is provided in Fig. 2. (Values are given in degrees where vertical = 0°, increasing clockwise).

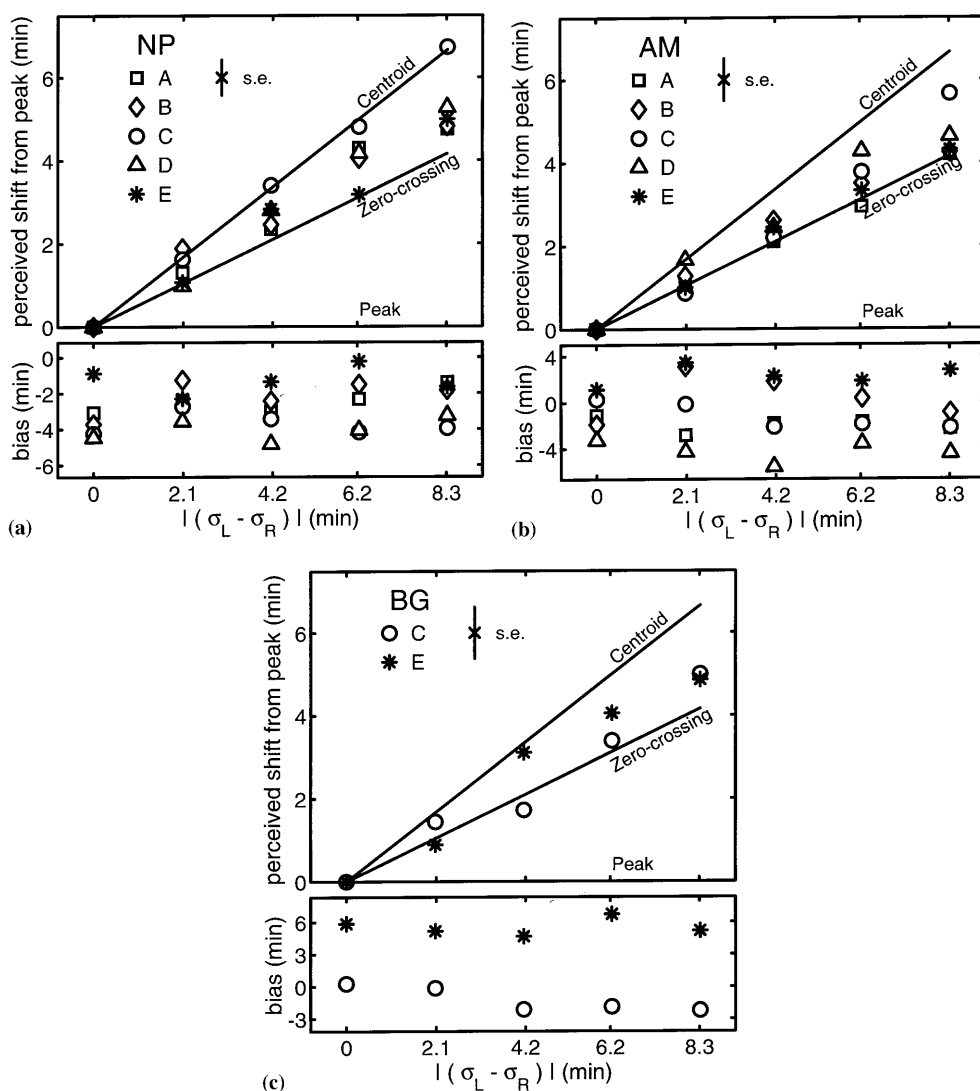


Fig. 3. Perceived position of the target OM relative to the reference OM as a function of the degree of asymmetry of the target OM ($|\sigma_L - \sigma_R|$) for each of the observers (upper panels), together with the positions of the centroid, zero-crossing midpoint, and the peak. Also presented for each observer is the response bias (lower panels). The standard error bars represent the average standard error across conditions. Each data point is based on 12 PEST staircases for NP, and 6 PEST staircases for AM and BG.

determining the location of the maximum value in the filter response (Fig. 1F). Best fits are indicated in Fig. 4 by the solid lines. Fig. 5 depicts the corresponding receptive field profiles, together with the numerical estimates of σ_1 and σ_2 . The corresponding values for the width of the excitatory centre (w_c) were found to be 1.24, 0.89 and 0.98° for observers NP, AM, and BG, respectively (mean = 1.04°). Kingdom and Keeble (1999) established that the sensitivity to particular frequencies of OM is scale invariant, that is, tied to the spatial frequency of the carrier pattern. Consequently, an appropriate metric for comparison is in terms of the number of carrier cycles covered by the receptive field excitatory centre. The excitatory centre as estimated from the present data covers about 13 carrier cycles ($1.04 \times 12.6 \text{ cyc deg}^{-1}$), which is very similar to

the value of 14 obtained by Kingdom and Keeble (1996).

Another remarkable similarity between our estimated receptive field profiles and the profiles as estimated by Kingdom and Keeble (1996) concerns the shape of the receptive field profiles. We replicated in our estimates the exceptionally shallow and broad surround regions of the profiles found by Kingdom and Keeble. This is in marked contrast to the receptive field profiles proposed for the detection of first-order structure in which the inhibitory regions are modelled as narrow and relatively deep (e.g. Marr & Ullman, 1981; Daugman, 1985). Shallow inhibitory regions are, however, consistent with the response properties of neurones measured beyond their classical receptive fields (Fiorani, Rosa, Gattass & Rocha-Miranda,

1992; Gattass et al., 1992; Li & Li, 1994), for example, when their classical receptive regions are masked or stimulated maximally (as would occur when presented with a large textured region). It has been shown that the function of these integrative regions is to modulate the response of a neurone in an inhibitory or excitatory fashion. The implication of this is that one may not

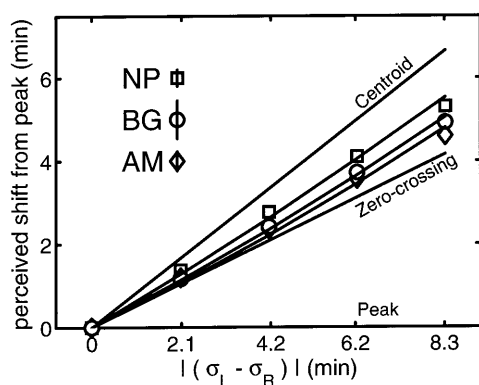


Fig. 4. Results averaged across stimulus configurations for each of the observers, together with the positions of the centroid, zero-crossing average, and the peak. Best fits to the data based on an interpretation of the data in terms of orientation-opponent filters are also presented for each observer individually. These fits were obtained by estimating the two spatial constants of a Difference-of-Gaussian shaped receptive-field profile resulting in a remarkably similar estimate of the RF profile as that obtained by other researchers. The error bars in the legend represent the average standard error for each observer.

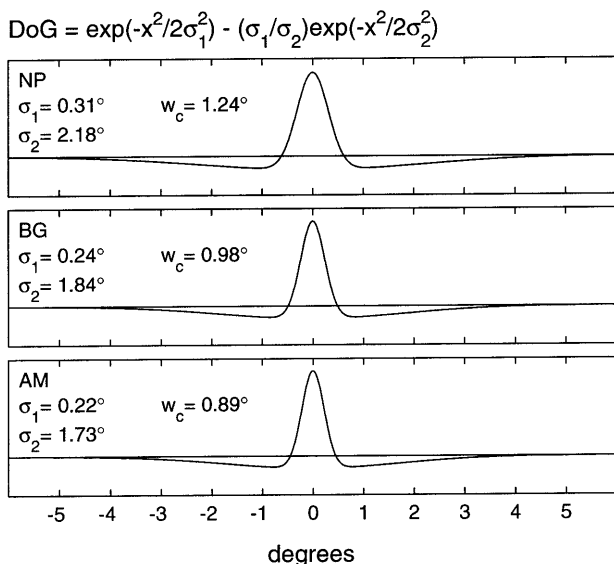


Fig. 5. The estimated receptive field profiles for the three observers. Receptive field profiles were modelled with a Difference-of-Gaussians (DoG) function. The estimates for the two spatial constants (σ_1 and σ_2) are indicated in the figure, along with the corresponding width of the excitatory centre of the profile (w_c). Our estimates show a remarkable similarity with those obtained by Kingdom and Keeble (1996) both in terms of the values for w_c and the overall shape of the profiles.

need to attribute OM detection and localisation to higher-level integrative processes, but rather to the operation of simple or complex cells of V1 with large inhibitory integrative regions.

It should be noted that our model is based on the orientation distribution used to generate the stimuli rather than on the distribution of neural activity as generated by the first stage of filtering. As such, our estimated receptive-field profiles incorporate the transfer characteristics of both the first and second-stage of the model. The profile can be taken to reflect that of the second-stage proper only to the extent to which the first stage of filtering results in a distribution of neural activity which accurately mirrors the stimulus generating function. To demonstrate that it is not unreasonable to assume that this is indeed the case, we filtered the textures displayed in Fig. 1A with a Gabor filter with relative spatial dimensions as proposed by Daugman (1980), followed by full-wave rectification. The Gabor filter was matched to the spatial frequency of the stimuli and the peak orientation of the orientation modulation. We have superimposed the results, averaged within the vertical columns, onto the stimulus-generating functions in Fig. 1B and show that the profiles, extracted in this manner from the filtered images, follow their generative functions closely. It should also be noted that the assumption that the distribution of neural activity accurately reflects the stimulus-generating function is not crucial to the model. Modest systematic discrepancies between the stimulus and neural response can be compensated for by minor modifications in the parameter estimates of the second-stage receptive-field profile.

An alternative explanation of our results, deserving some attention, would be in terms of a weighted average of the position of the centroid of the OM with the position of the zero-crossing and/or peak of the distribution. The weighted average would be of the form:

$$P_G = (1 - \alpha - \beta) P_C + \alpha P_{Z/C} + \beta P_P$$

$$0 \leq \alpha \leq 1 - \beta \quad \text{and} \quad 0 \leq \beta \leq 1 - \alpha \quad (2)$$

where P_G is the perceived global position of the OM, and P_C , $P_{Z/C}$, and P_P are the positions of the centroid, zero-crossings and peak of the OM, respectively. Eq. (2) would fit the data about equally well as the fit obtained with Kingdom and Keeble's operators. However, there are two problems associated with this interpretation. First, this approach would lead only to a family of solutions for α and β ; it cannot be determined whether the zero-crossings or the peak produced the deviation from the centroid prediction. Second, and perhaps more importantly, an explanation in terms of Eq. (2) would merely be descriptive in nature; it is not at all obvious how the position of either the centroid, zero-crossing, or peak of the OM would be determined by the visual system.

The results of alignment studies employing luminance-modulated (LM) stimuli have been interpreted in terms of the locations of the centroid, zero-crossing, and peak, among other local features, of the luminance distribution (Akutsu et al., 1999; Badcock et al., 1996; Hess & Holliday, 1992, 1996; Hess & Hayes, 1994; Whitaker et al., 1996; Whitaker & McGraw, 1998). Although such an interpretation is interesting from a functional perspective, it does little to elucidate the underlying processes involved. Gray and Regan (1998) established that the frequency response function of LM stimuli is similar to that of OM stimuli, at least at low spatial frequencies. This suggests that the results of alignment studies with LM stimuli might also be interpreted in the context of the receptive field shape of positionally-labelled neurones. This approach offers the possibility of reconciling the results of previous studies of LM localisation, particularly where results have been shown to lie midway between predictions based on local features.

In summary, our results demonstrate that observers are sensitive to the location of global distributions of orientation. Furthermore, an interpretation of our results can be made on the basis of orientation-contrast detectors, with the best fit to our results achieved with detectors of spatial dimensions remarkably similar to those estimated previously by Kingdom and Keeble (1996) using an entirely different task, different stimulus parameters and configurations.

Acknowledgements

This research was supported by a grant from the Australian Research Council. We wish to thank Dr David Badcock for helpful suggestions.

References

- Akutsu, H., McGraw, P. V., & Levi, D. M. (1999). Alignment of separated patches: multiple location tags. *Vision Research*, *39*, 789–801.
- Arsenault, A. S., Wilkinson, F., & Kingdom, F. A. A. (1999). Modulation frequency and orientation tuning of second-order texture mechanisms. *Journal of the Optical Society of America A*, *16*, 427–435.
- Badcock, D. R., Hess, R. F., & Dobbins, K. (1996). Localization of element clusters: multiple cues. *Vision Research*, *36*, 1467–1472.
- Daugman, J. G. (1980). Two-dimensional spectral analysis of cortical receptive field profiles. *Vision Research*, *20*, 847–856.
- Daugman, J. G. (1985). Uncertainty relation for resolution in space, spatial frequency, and orientation optimised by two-dimensional visual cortical filters. *Journal of the Optical Society of America A*, *2*, 1160–1169.
- Fiorani Jr, M., Rosa, M. G. P., Gattass, R., & Rocha-Miranda, C. E. (1992). Dynamic surrounds of receptive fields in primate striate cortex: a physiological basis for perceptual completion? *Proceedings of the National Academy of Sciences USA*, *89*, 8547–8551.
- Gattass, R., Fiorani Jr, M., Rosa, M. G. P., Piñon, M. C. G. P., De Sousa, A. P. B., & Soares, J. G. M. (1992). Visual responses outside the classical receptive field in primate striate cortex: a possible correlate of perceptual completion. In: R. Lent, *The visual system from genesis to maturity* (pp. 233–244). Boston, MA: Birkhäuser.
- Gray, R., & Regan, D. (1998). Spatial frequency discrimination and detection characteristics for gratings defined by orientation texture. *Vision Research*, *38*, 2601–2617.
- Hess, R. F., & Holliday, I. E. (1992). The coding of spatial position by the human visual system: Effects of spatial scale and contrast. *Vision Research*, *32*, 1085–1097.
- Hess, R. F., & Holliday, I. (1996). Primitives used in spatial localization of nonabutting stimuli: peaks or centroids. *Vision Research*, *36*, 3821–3826.
- Hess, R. F., & Hayes, A. (1994). The coding of spatial position by the human visual system: effects of spatial scale and retinal eccentricity. *Vision Research*, *34*, 625–643.
- Kingdom, F. A. A., & Keeble, D. R. T. (1996). A linear systems approach to the detection of both abrupt and smooth spatial variations in orientation-defined textures. *Vision Research*, *36*, 409–420.
- Kingdom, F. A. A., & Keeble, D. R. T. (1999). On the mechanism for scale invariance in orientation-defined textures. *Vision Research*, *39*, 1477–1489.
- Kingdom, F. A., Keeble, D., & Moulden, B. (1995). Sensitivity to orientation modulation in micropattern-based textures. *Vision Research*, *35*, 79–91.
- Knierim, J. J., & Van Essen, D. C. (1992). Neuronal responses to static texture patterns in area V1 of the alert macaque monkey. *Journal of Neurophysiology*, *67*, 961–980.
- Levi, D. M., & Klein, S. A. (1990). Equivalent intrinsic blur in spatial vision. *Vision Research*, *30*, 1971–1993.
- Li, C.-Y., & Li, W. (1994). Extensive integration field beyond the classical receptive field of cat's striate cortical neurons-classification and tuning properties. *Vision Research*, *34*, 2337–2355.
- Lotze, H. (1885). *Microcosmos*. Edinburgh: T and T Clarke (E. Hamilton, & E.E. Constance-Jones, Trans.).
- Marr, D., & Ullman, S. (1981). Directional selectivity and its use in early visual processing. *Proceedings of the Royal Society of London, B*, *211*, 151–180.
- Morgan, M. J., & Glennerster, A. (1991). Efficiency of locating centres of dot-clusters by human observers. *Vision Research*, *31*, 2075–2083.
- Olavarria, J. F., DeYoe, E. A., Knierim, J. J., Fox, J. M., & Van Essen, D. C. (1992). Neural responses to visual texture patterns in middle temporal area of the macaque monkey. *Journal of Neurophysiology*, *68*, 164–181.
- O'Shea, R. P., & Mitchell, D. E. (1990). Vernier acuity with opposite-contrast stimuli. *Perception*, *19*, 207–221.
- Pentland, A. (1980). Maximum likelihood estimation: the best PEST. *Perception & Psychophysics*, *28*(4), 377–379.
- Toet, A., & Koenderink, J. J. (1988). Differential spatial displacement discrimination thresholds for Gabor patches. *Vision Research*, *28*, 133–143.
- Waugh, S. J., & Levi, D. M. (1993). Visibility, timing and vernier acuity. *Vision Research*, *33*, 505–526.
- Westheimer, G. (1981). *Visual hyperacuity: Progress in sensory physiology, vol 1* (pp. 1–30). New York: Springer.
- Westheimer, G., & McKee, S. P. (1977). Spatial configurations for visual hyperacuity. *Vision Research*, *17*, 941–947.
- Whitaker, D., McGraw, P. V., Pacey, I., & Barrett, B. T. (1996). Centroid analysis predicts visual localization of first- and second-order stimuli. *Vision Research*, *36*, 2957–2970.
- Whitaker, D., & McGraw, P. V. (1998). Geometric representation of the mechanisms underlying human curvature detection. *Vision Research*, *38*, 3843–3848.